Polyethylene glycol assisted facile sol-gel synthesis of lanthanum oxide nanoparticles

Kabir, Humayun; Nandyala, Sooraj Hussain; Rahman, M. Mahbubur; Kabir, Md Alamgir; Pikramenou, Zoe; Laver, Mark; Stamboulis, Artemis

DOI:
10.1016/j.ceramint.2018.09.183

Document Version
Peer reviewed version

Citation for published version (Harvard):
Kabir, H, Nandyala, SH, Rahman, MM, Kabir, MA, Pikramenou, Z, Laver, M & Stamboulis, A 2019, 'Polyethylene glycol assisted facile sol-gel synthesis of lanthanum oxide nanoparticles: structural characterisation and photoluminescence studies', *Ceramics International*, vol. 45, no. 1, pp. 424-431. https://doi.org/10.1016/j.ceramint.2018.09.183

Figure

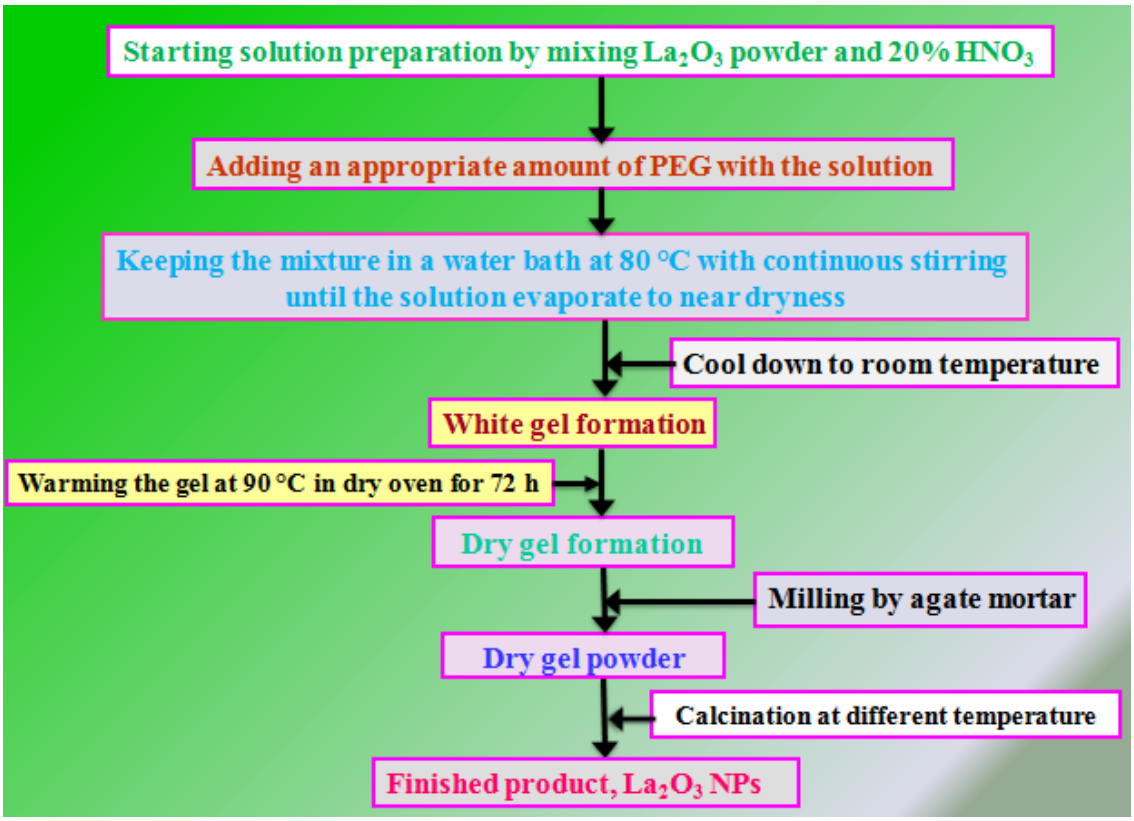

Fig. 1. Flow chat of the synthesis process.

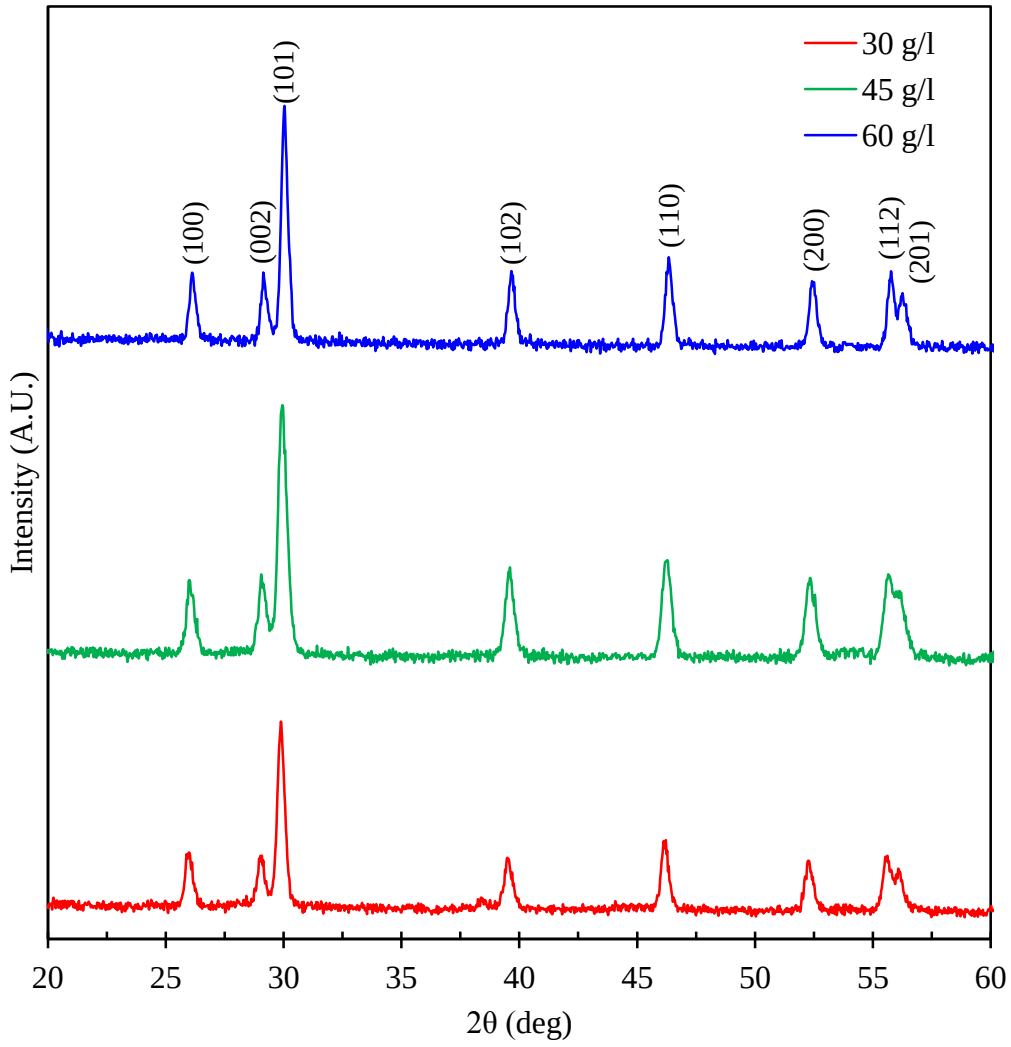

Fig. 2. XRD patterns of La_2O_3 NPs samples with PEG concentration 30 g/l, 45 g/l, and 60 g/l.

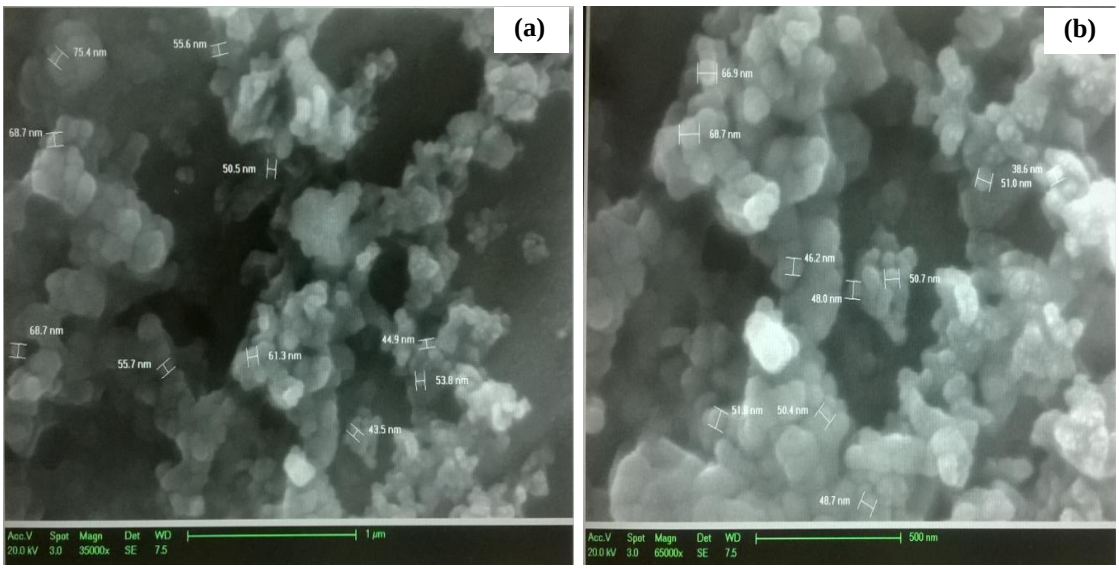

Fig. 3. SEM micrographs of La_2O_3 NPs sample with PEG concentration 30 g/l at magnification (a) 35k×, (b) 65k×.

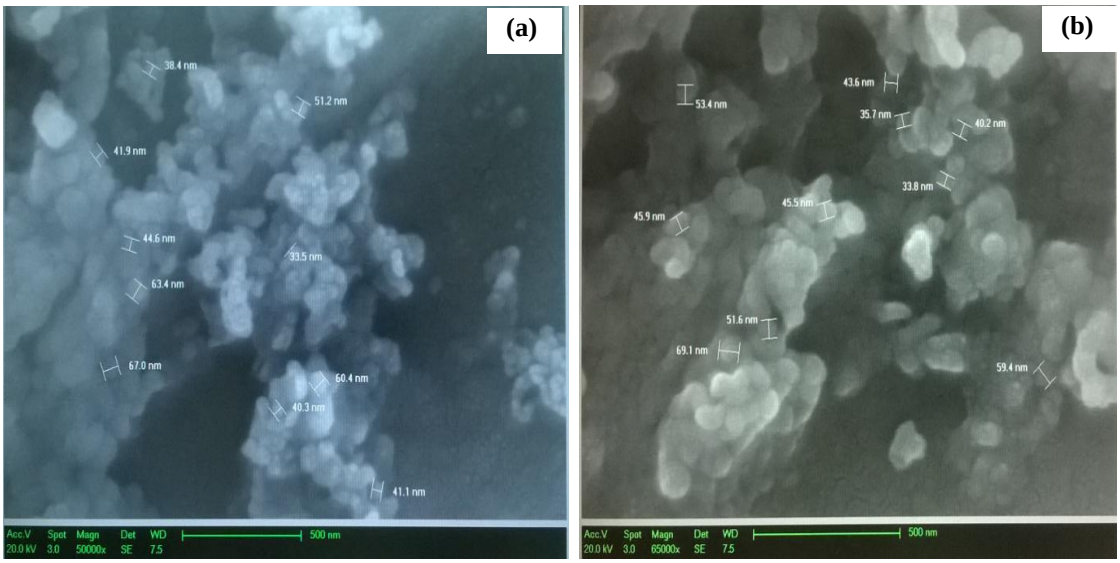

Fig. 4. SEM micrographs of La_2O_3 NPs sample with PEG concentration 45 g/l at magnification (a) 50k×, (b) 65k×.

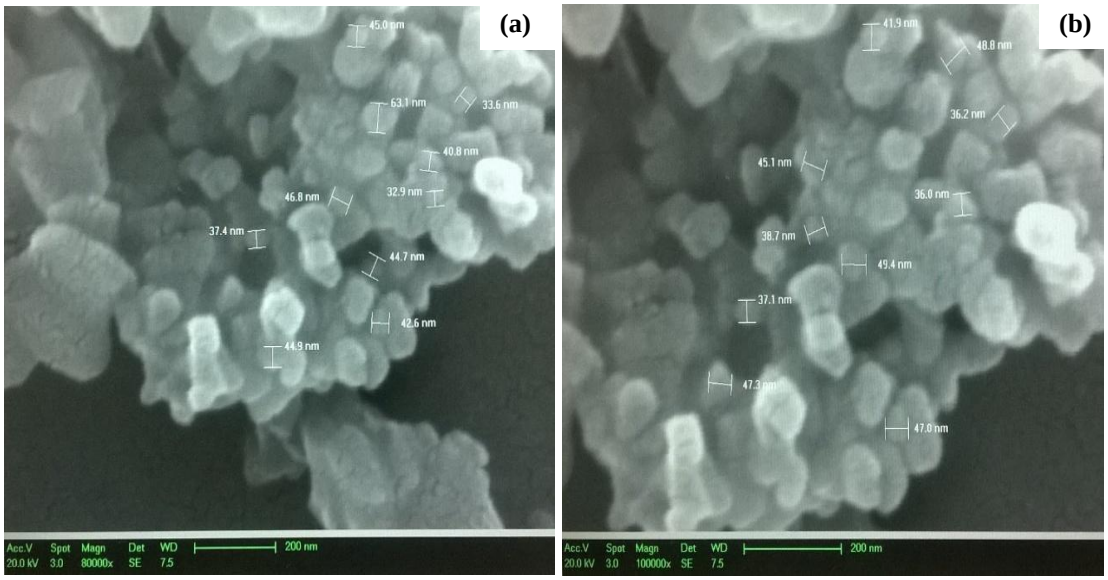

Fig. 5. SEM micrographs of La_2O_3 NPs sample with PEG concentration 60 g/l at magnification (a) 80k×, (b) 100k×.

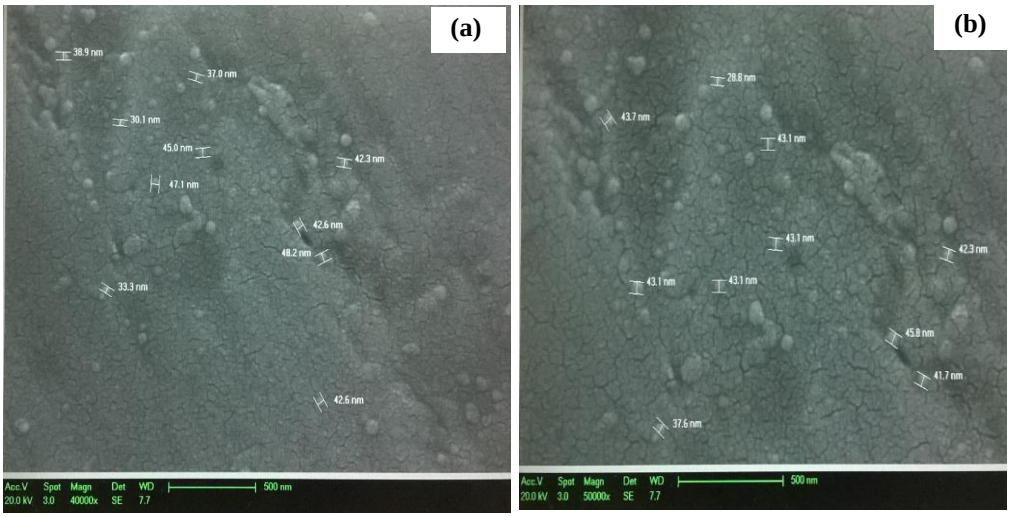

Fig. 6. SEM micrographs of dispersed La_2O_3 NPs sample with PEG concentration 30 g/l at magnification (a) 40k×, (b) 50k×.

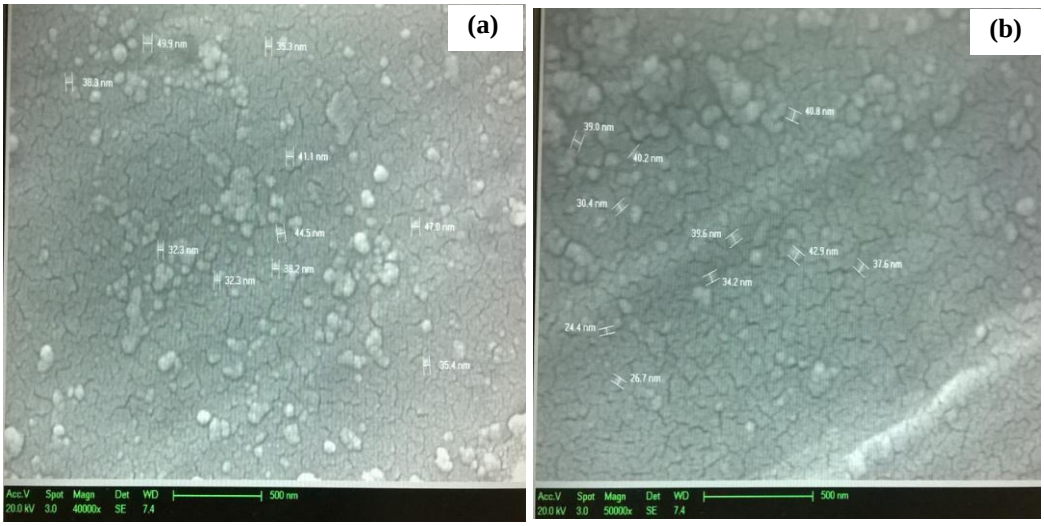

Fig. 7. SEM micrographs of dispersed La_2O_3 nanoparticles sample with PEG concentration 45 g/l at magnification (a) 40k×, (b) 50k×.

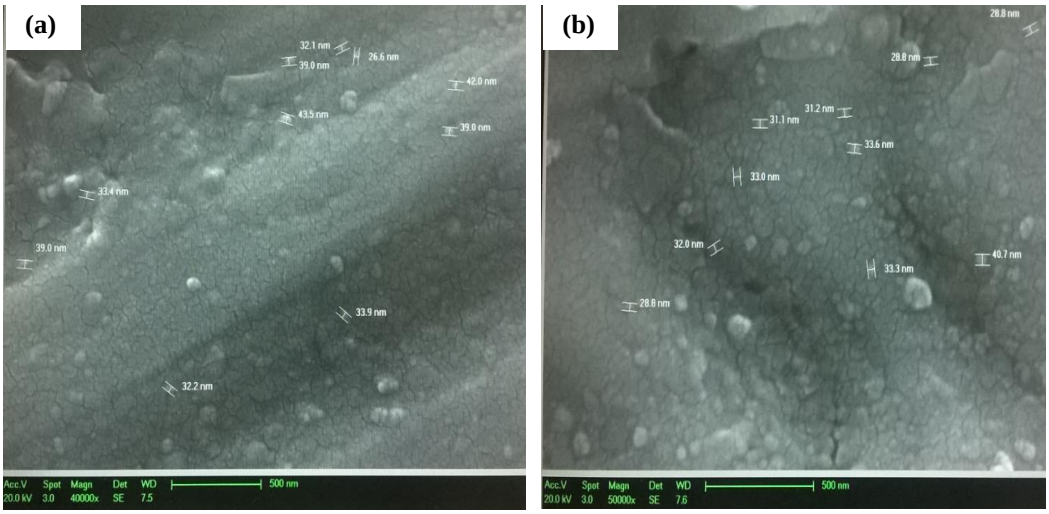

Fig. 8. SEM micrographs of dispersed La_2O_3 nanoparticles sample with PEG concentration 60 g/l at magnification (a) 40k×, (b) 50k×.

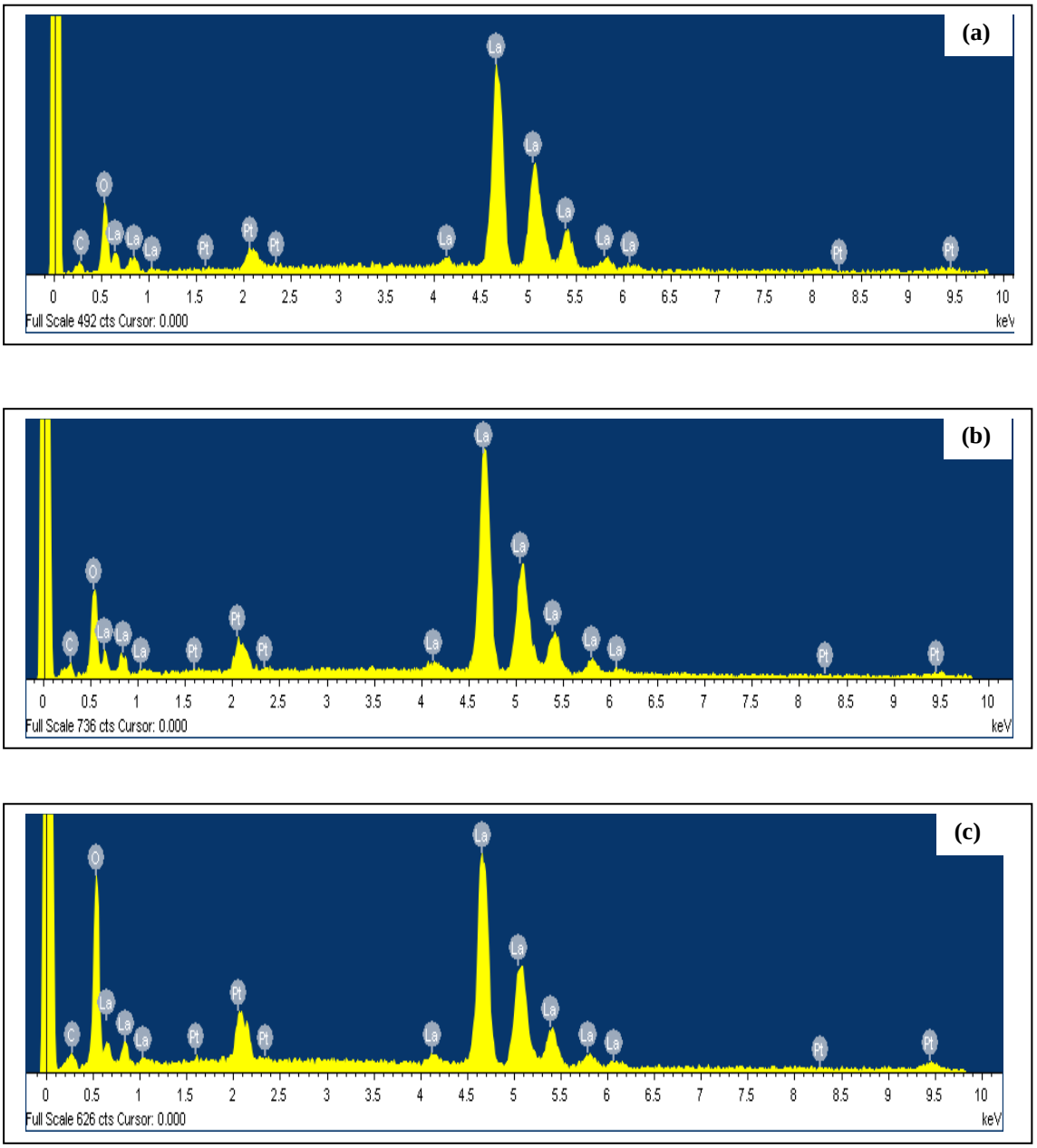

Fig. 9. EDS spectra of different samples of La_2O_3 NPs sample with PEG concentration (a) 30 g/l, (b) 45 g/l and (c) 60 g/l.

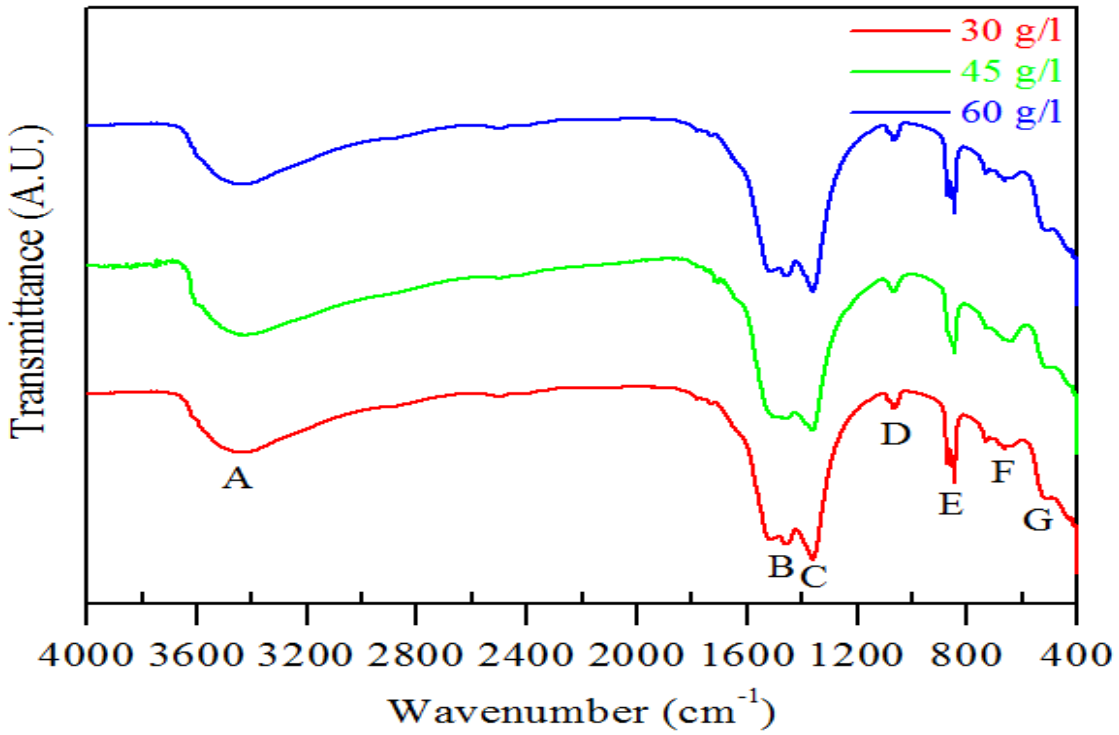

Fig. 10. FTIR spectra of La_2O_3 NPs samples with different PEG concentrations.

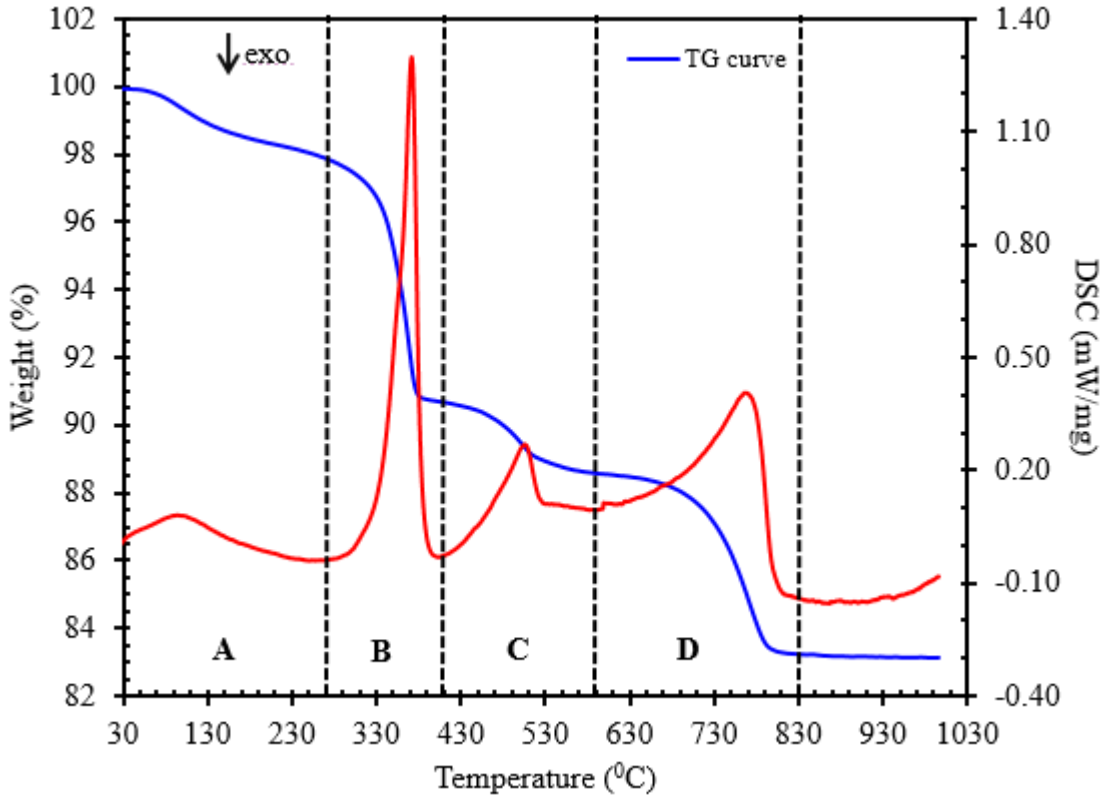

Fig. 11. TG-DSC traces of the lanthanum compound dried gel powder prepared at PEG concentration of 60 g/l.

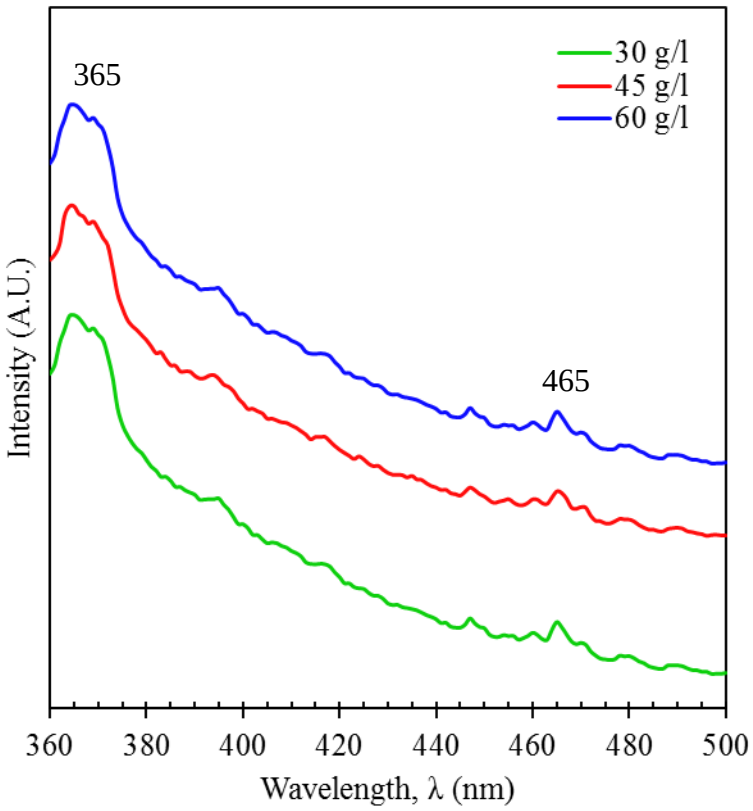

Fig. 12. PL spectra of different La_2O_3 NPs samples at varied PEG concentrations.

Table

Table 1. Determination of interplanar distance and lattice constants of La_2O_3 NPs.

Sample (PEG concen-tration)	Interplanar distance, d_{hkl} (Å)			Lattice constants, a and b (Å)			Lattice constants, c (Å)			Average values of a or b (Å)	Average of c (Å)
	(100)	(002)	(110)	(100)	(002)	(110)	(100)	(002)	(110)		
30 g/l	3.4449	3.0787	1.9680	3.9778	3.9518	3.9360	6.0317	6.1573	6.2393	3.9552	6.1428
45 g/l	3.4326	3.0750	1.9655	3.9636	3.9433	3.9310	6.0505	6.1499	6.2133	3.9460	6.1379
60 g/l	3.4144	3.0750	1.9595	3.9426	3.9274	3.9190	6.0741	6.1499	6.1936	3.9297	6.1392

Table 2. Crystallographic parameters of La_2O_3 NPs.

Sample	Crystallite size, D (nm)	Lattice strain, ε	Dislocation density, δ	Unit cell volume, V(Å^3)	Crystal index, C_i	c/a ratio
30 g/l	28.32	0.0050	0.1001	83.2191	3507.06	1.5531
45 g/l	27.89	0.0051	0.0983	82.7655	4865.94	1.5555
60 g/l	25.37	0.0055	0.1081	82.0993	4056.49	1.5623

Table 3. Average particle size for different samples of La_2O_3 NPs:

Sample	Magnification(k×)	Particle size (nm)	Average particle size (nm)
30 g/l	35	57.8	55.0
	65	52.1	
45 g/l	50	48.2	48.0
	65	47.8	
60 g/l	80	43.2	43.0
	100	42.8	

Table 4. Average particle size for different dispersed samples of La_2O_3 NPs:

Sample	Magnification(k×)	Particle size (nm)	Average particle size (nm)
30 g/l	40	40.7	41.0
	50	41.2	
45 g/l	40	39.4	37.5
	50	35.6	
60 g/l	40	36.1	34.1
	50	32.1	

Table 5. The weight percentage (wt. %) of the different elements present in different samples of La_2O_3 NPs.

Sample	Element present in Wt%		
	La	O	C
30 g/l	77.69	16.98	5.33
45 g/l	73.87	20.42	5.71
60 g/l	59.83	34.04	6.13

Table 6. Assignments of FTIR absorption peaks for La_2O_3 nanoparticles samples NP750-30, NP750-45 and NP750-60.

Assignments	Wavenumber (cm^{-1})		
	As prepared La_2O_3 nanoparticles		
	30 g/l	45 g/l	60 g/l
O-H stretching vibration (A)	3424	3421	3424
Asym. stretching of COO^- (B)	1509, 1459	1456	1510, 1460
Symmetric stretching of COO^- (C)	1363	1362	1363
C-O stretching vibration (D)	1067	1067	1067
C-O bending vibration (E)	855, 846	845	856, 845
La-O stretching vibration (F)	678	676	678
La–O bending vibration (G)	509	511	510

Polyethylene glycolassisted facile sol-gel synthesis of lanthanum oxide nanoparticles: Structural characterizations and photoluminescence studies

Humayun Kabir[a, b], Sooraj Hussain Nandyala[a], M Mahbubur Rahman[b,c], Md Alamgir Kabir[a,b,e], Zoe Pikramenou[d], Mark Laver[a], Artemis Stamboulis[a]

[a]*School of Metallurgy and Materials, University of Birmingham, Edgbaston, Birmingham, B15 2TT, UK.*

[b]*Department of Physics, Jahangirnagar University, Savar, Dhaka-1342, Bangladesh.*

[c]*Surface Analysis & Materials Engineering Research Group*

School of Engineering & Information Technology, Murdoch University, Murdoch, WA 6150, Australia

[d]*School of Chemistry, University of Birmingham, Edgbaston, Birmingham, B15 2TT, UK.*

[e]*Department of Physics, Kent State University , Kent, Ohio 44243, USA.*

Corresponding author: H Kabir (rumy140@juniv.edu)

ABSTRACT

In this work, lanthanum oxide nanoparticles (La_2O_3 NPs) synthesised *via* facile sol-gel method, using micro-sized lanthanum oxide powders, 20% nitric acid and high molecular weight polyethylene glycol (PEG), were characterised using X-ray diffraction (XRD), environmental scanning electron microscopy (ESEM), energy-dispersive X-ray (EDAX) spectroscopy, Fourier transform infrared (FTIR) spectroscopy, thermogravimetric analysis (TGA),differential scanning calorimetry (DSC), and photoluminescence (PL) spectroscopy. Our findings indicated that the concentration of PEG strongly influence the particle size and lattice strain of the La_2O_3 NPs. Single phase hexagonal crystal structure was confirmed *via* XRD studies with lattice constants, $a = b =$ 0.3973 nm and $c = 0.6129$ nm. The average crystallite size and lattice strain estimated were in the range of 25.37-28.32, nm and 0.0050-0.0055, respectively. An increment nature of the crystallinity and lattice strains of the NPs were observed with the subsequent enhancement of PEG-contents, while the average particle size was reduced. The average crystallite size of La_2O_3 NPs estimated from ESEM imaging was in good agreement with that obtained from the XRD data. The photoluminescence spectra revealed a strong emission band located at a wavelength of 364 or 365 nm (typical green band) for all La_2O_3NP samples. This is ascribed to the recombination of delocalized electronsaround the conduction band with a single charged state of a surface oxygen vacancy.

Keywords: Sol-gel method, X-ray diffraction, particle size, lattice strain, lattice constant, photoluminescence.

1. Introduction

Applications of nanoparticles (NPs) in nanoengineering and nanotechnology is a fast developing area of research in science and technology due to a large number of unique properties which are not present in bulk materials. Rare earth based metal oxide (ReMO) NPs have wide spread applications in microelectronic circuits, piezoelectric devices, dielectric resonators, sensors, fuel cells, colouring agents, additives for various alloys and polymers, coatings, dopants, oxygen pumps, polishing media, flat-panels and field-emission displays, CRT screens, infrared and ultraviolet absorbents, catalysts and catalyst supports [1-3]. The ReMOs are also used as electrodes, light-emitting devices, hydrogen storage, laser, and piezoelectric materials among others. In the course of the combustion of fossil fuels, large species of CO, NO_x, and SO_x are created which can be removed using ReMONPs [4-6]. Among the existing ReMOs, lanthanum oxide (La_2O_3) possesses many interesting properties such as large band-gap (4.3 eV), minimum lattice energy, and exceptionally high dielectric constant [7, 8]. Consequently, lanthanum oxide nanoparticles have potential uses in rechargeable batteries, fuel cells, catalysts, optical devices, magnetic storage, MRI, dielectric layers, gas sensors, biosensors, biomedicine, optical coating, photoelectric conversion, and catalysis [9-13].

Lanthanum oxide NPs, nanorods, nanowires and nanosheets can be prepared using various chemical and physical techniques including hydrothermal [14, 15], solvothermal [16], microwave [16, 17], sol–gel [17, 18], sonochemical [19-21], and reveres micelles [22].Amongst these methods, the sol-gel synthesis process is a facile, inexpensiveand does not require any sophisticated, complicated and specialist equipment. Hydrothermal synthesis of lanthania nanoparticles was reported by Goharshadi *et al.* [23] and an average particle size below 30 nm was achieved. Sol-gel synthesis of lanthanum barium copper oxide nanoparticles was carried out by S. Khanahmadzadeh *et al.* [24], and the nanostructure of the as synthesised nanoparticles were confirmed using XRD (28 nm) and SEM (67 nm) studies. Authors also demonstrated that the nanoparticles show a significant level of photocatalytic activity. The La_2O_3 hierarchical micro/nanostructures prepared by Liu *et al.* [25] showed that the morphology of La_2O_3 micro/nanostructures can be controlled by changing concentration of the reactants, reaction temperatures, and cooling treatment procedure. It was also established that La_2O_3 micro/nanostructures can be used to remove phosphate from microbial growth media and have potential application prospects in water pollution of eutrophication, or reduction ofexcess phosphate from human body in biomedical areas. L. Zhang *et al.* [26] studied the toxicity of lanthanum oxide (60-80 nm) and silver oxide (10-40 nm) nanoparticles to the fungus *Moniliellawahieum* $Y12^T$. Their studies indicated that silver oxide nanoparticles can be a nonspecific inhibitor for the treatment of *M. wahieum* $Y12^T$, a eukaryotic biodiesel contaminant.

This clearly indicates that lanthanum oxide has a lot of potential to be used in biomedicine, photocatalysts, and gas sensors. Thus exploration of a simple, inexpensive, environmental friendly technique to synthesize high quality La_2O_3nanoparticles may always remain in the focus.

In view of these, in this work we employed a simple sol-gel technique to synthesis nanometer-sized La_2O_3 ultrafine particles using micro-sized lanthanum (III) oxide powders, 20% nitric acid and polyethylene glycol. The structural, chemical, thermal, and photoluminescence properties of La_2O_3 nanoparticles were correlated *via* X-ray powder diffraction, environmental scanning electron microscope, FTIR spectroscopy, TG and DSC analysis, and photoluminescence spectroscopic studies. The effect of concentration of polyethylene glycol on the average particle size of the La_2O_3 nanoparticles was reported.

2. Experimental details

2.1 Sol-gel synthesis of La_2O_3 NPs

Micro-sized (Max. 200 μm) lanthanum (III) oxide powder (ARGrade, Sigma Aldrich, UK), 20% nitric acid (Certified Grade, LabChem Inc., USA), and high molecular weight (20000) polyethylene glycol (Sigma Aldrich, UK) were used as raw materials, complexing agent, and surfactant, respectively. All these chemicals were used in received forms. Initially 2 g micro-sized La_2O_3 powders in a pre-cleaned glass beaker. 18.5 ml 20% aqueous solution of HNO_3 was drop wise added to the La_2O_3 powders with continuous and vigorous magnetic stirring until the entire La_2O_3 powders reacted with HNO_3 to produce an aqueous solution of lanthanum nitrate ($La(NO_3)_3.6H_2O$). Then different amounts of PEG were added to produce a solution with different PEG concentrations, such as 30 g/l, 45 g/l, 60 g/l and 70 g/l. The resultant solution was further stirred for 15 minutes using a magnetic stirrer. The solution was then kept in a water bath at 80 °C with continuous stirring for approximately 2 h until most of the water was evaporated and a clear gel is formed. The gel was allowed to cool down to room temperature. Thereafter, the clear gel was placed in an oven at 90 °C for 72 h to form a dry gel. Using an agate mortar and pestle the dry gel was grounded to convert them to white powders. In order to remove the organic phases and to decompose the $La(NO_3)_3$, the obtained powders were heat treated at 300 °C. Finally, the resultant powders (La_2O_3 NPs) were calcined at a temperature of 750 °C. The flow chart given in Figure 1, describes the entire chemical procedure of sol-gel synthesis process of producing La_2O_3 NPs.

2.2 Characterization of Samples

The XRD measurements of La_2O_3 NPs were conducted for structural characterizationusing an Equinox 3000 X-ray powder diffractometer in the 2θ range from 10 to 60°, in steps of 0.03°.

The XRD machine uses graphite monochromatic Cu-K_α radiation (λ = 0.154 18 nm) at operating voltage of 35 kV and current of 25 mA. XRD measurements were done at room temperatures.

The surface morphology and particle size of La_2O_3 NPs were measured using a Philips XL 30 ESEM equipped with Oxford INCA EDX FEG electron microscope operated at 20 kV at different magnifications. The analysis was performed on the SEM mode in a high vacuum condition. To prepare a sample for ESEM, 1.0 mg of La_2O_3 NPs was suspended in 5.0 ml of ethanol and bath-sonicated for 20 minutes using an ultra-sonication bath (FB15046, Fisherbrand). A drop of the resulting solution was placed onto a thin Cu coatedfilm set on a steel stab. The EDS of the samples was performed by a Philips XL 30 ESEM and EDX FEG electron microscope operated at 10 kV at different magnifications.

The FTIR spectra of La_2O_3 NPs were recorded in transmittance (%) mode at room temperature using a double beam IR spectrophotometer (Nicolet 8600 FTIR spectrometer) in the wavenumber range from 400 to 4000 cm^{-1}. To obtain the IR spectra, a ratio of 1:100 of the sample and potassium bromide, KBr were used. The background using a control sample of KBr was always taken prior to each measurement. The applied resolution and number of scan was 4 cm^{-1} and 100 per minute, respectively.

TG and DSC analysis of the as synthesized La_2O_3 NPs were carried out from room temperature to 1000 °C at a heating rate of 10 °C/min under Ar gas flow by a NETZSCH Thermal Analysis STA 449C with pairs of matched platinum-rhodium crucibles.

The PL spectra La_2O_3 NPs were collected by a QuantaMaster^{TM} 510 spectrofluorometer (HORIBA JobinYvon GmbH, Hauptstrasse 1, 82008 Unterhaching, Germany) equipped with a Xe lamp light source for excitation (with excitation wavelength, λ_{ex} = 300 nm) at room temperature.

3. Results and discussion

3.1. Detail structural analysis of La_2O_3 NPs via XRD measurements

X-ray diffraction patterns of La_2O_3 NPs with different PEG concentrations shown in Figure 2 reveal the overall crystal structure and phase purity of the synthesised La_2O_3 NPs. The strong and sharp diffraction peaks also confirm the good crystallinity of the La_2O_3 NPs. The diffraction peaks of the La_2O_3 NPs indexed to (100), (002), (101), (102), (110), (200), (112), and (201) reflections planes are corresponding to the hexagonal crystal symmetry with a space group *P*63/*mmc* (194), and lattice constants of $a = b$ = 0.3973 nm, and c = 0.6129 nm (JCPDS card No. 83-1348). Absence of any additional diffraction peaks it indicates the high purity of La_2O_3 NPs. The strongest broadest diffraction peak at (101) reflection plane is obtained for the La_2O_3 NPsamples with a PEG concentration of 60 g/l.

The lattice constants, *a* and *c* of for hexagonal La_2O_3 NPs were calculated by the following equation [27],

$$\frac{1}{d_{hkl}^2} = \frac{4}{3}\left(\frac{h^2 + hk + k^2}{a^2}\right) + \frac{l^2}{c^2} \qquad (1)$$

where d_{hkl} is the inter-planar spacing of the atomic planes and (*hkl*) is Miller indices. The estimated lattice parameters are tabulated in Table 1. The lattice constant values reported in these studies are in good agreement with that testified in [28].

The peak broadening in XRD patternsis associated with both the instrumental and sample factors. Thus, it is necessary to make a correction of the peak broadening due to instrumental factor first. The remaining broadening is then ascribed to sample related factors which include broadening due to the crystallite size and strain. The corrected broadening of the diffraction peak (β_C) can be determined by the following relation,

$$\beta_C^2 = \beta_M^2 - \beta_I^2 \qquad (2)$$

where β_M and β_I are the measured broadening due to sample and that of the instrument, respectively.

The peak broadening can occur for very a tiny crystallite, and the width of a diffraction peak varies with the crystallite size of the samples. The crystallite size can be calculated using the Scherrer's formula [29],

$$D = \frac{K\lambda}{\beta cos\theta_B} \qquad (3)$$

where *D* is the diameter of the crystallite, β is the full width at half maximum (FWHM) of the selected diffraction peak, θ_B is the Bragg diffraction angle, λ is the X-ray wavelength, and *K* is a constant of which the value depends on the shape of the crystallite. The value of K is equal to 0.9 for spherically shaped crystals. The FWHM of the XRD peaks may also contain contributions from lattice strain, ε_{str} and the strain induced in powders owing to crystal imperfection and distortion can be calculated using the Stokes-Wilson equation [30],

$$\varepsilon_{str} = \frac{\beta_C}{4\ tan\theta} \qquad (4)$$

The values of average crystallite size and lattice strain determined using Equations (3) and (4) are organized in Table 2. From Table 2, we see that the average crystallite size decreases while lattice strain increases with the increased PEG concentration in the sol. similar features were reported by Wang *et al.* [31]. As the PEG concentration is enhances, the mean particle size of La_2O_3NPs is notably decreased due to the enhanced steric hindrance by the adsorption of PEG on La_2O_3 particle surfaces. This means that the PEG polymer surrounds the crystal nuclei of lanthanum nitrate, inhibits their growth, and thereby yields the steric hindrance effect resulting to shorten

agglomeration of the nanoparticles. When the concentration of PEG is inadequate to entirely conceal the crystal nuclei, the growth of crystal could not be impeded properly by adsorbing polymer which results larger particles. Therefore, the increased PEG concentration can successfully rise the degree of coverage on the crystal nuclei. Consequently, this will not only decrease the mean NPs size gradually, but also reduce the agglomeration of particle-particle around the sol-gel surface.

Properties of materials are strongly affected by crystallographic defects or irregularity within a crystal structure, known as dislocation. In crystalline solids, atoms or molecules exist in a repeated and periodic nature at fixed distancewhich can be found by a unit cell parameter.These regular patterns in a crystal are interrupted by dislocations. The dislocation density, δ of La_2O_3 NPs was calculated using the following expression [32],

$$\delta = \frac{15\beta\ cos\theta}{4aD} \qquad (5)$$

where symbols have their usual meanings.The unit cell volume, V of hexagonal La_2O_3 NPs was obtained using the following relation [33],

$$V = \frac{\sqrt{3}}{2}a^2c \qquad (6)$$

where a and c are the lattice constants of La_2O_3 NPs. The estimated values of δ and V of hexagonal La_2O_3 NPs are listed in Table 2. It is apparent that the La_2O_3 NPs with PEG concentration of 60 g/l has largest unit cell volume.The crystallinity of La_2O_3 NPs, represented by the crystal index, C_i and was calculated from XRD data using the following relation [34],

$$C_i = \frac{I_{max}}{\beta_c} \qquad (7)$$

where, $I_{max}$is the maximum intensity of the XRD peak and β_c is the value of corrected FWHM. The computed C_i values are also scheduled in Table 2.

3.2 Surface morphology of La_2O_3 NPs

The grain size, shape and surface morphology of the synthesised La_2O_3 NPs at various PEG concentration realized *via* ESEM micrographs, at different magnifications, are shown in Figures 3-5. It is seen that the La_2O_3 NPs are mostly agglomerated, porous and 3D nanoparticle superlattices having multiple facets [34].The particle size of La_2O_3 NPs at different magnifications for various samples is recorded in Table 3. It is also seen that the particle size of the La_2O_3 NPs decreased with the gradual increase in PEG concentrations. This decrease in particle size with the rise in PEG concentration is attributed to the enhanced steric hindrance bythe adsorption of polymer polyethylene glycol on the surfaces of La_2O_3 particles. This indicates that the PEG polymer surrounds the crystal nuclei of lanthanum nitrate and prevents their growth which creates

steric hindrance effect resulting to reduce particle-particle aggregation. However, if the PEG concentration is not enough to fully cover the crystal nuclei, the growth of crystal is not impeded effectively by adsorbing PEG. As a result, bigger particles will be acquired. On the other hand, if the PEG concentration rises, the coverage degree of PEG on the crystal nuclei is increased and consequently average particle size is delicately decreased. At the same time, the particle-particle agglomeration is gradually reduced [31].

In order to eliminate the particle agglomerations from the SEM images, the La_2O_3 nanoparticles were dispersed in ethanol and the effect of dispersion on the quality of SEM micrographs was studied. A total of 2.0 mg La_2O_3 NPs were dispersed in 5.0 mL of pure ethanol with the help of an ultrasonic bath (probe power level 3 and power density of 0.275 W/mL) for 20 min. Figures 6-8 show SEM micrographs of dispersed samples having PEG concentration of 30 g/l, 45 g/l, and 60 g/l, respectively at different magnifications. From Figures 6-8, we see that the uniformly dispersed La_2O_3 NPs have smaller diameters compared to the agglomerated ones presented in Figures 3-5. This happens due to the acoustic waves transmitted by ultra-sonication are effective in dispersing La_2O_3 NPs owing to the transient cavitation's and acoustic streaming that possibly redefines the shape and structure of NPs and change their surface morphologies [35]. The particle size for various La_2O_3 NP samples at different magnificationsis presented in Table 4. Again, we see that the particle size of La_2O_3 NPs is significantly decreased with the increased PEG-contents. This is related to the enhanced steric hindrance by the adsorption of PEG on the surfaces of La_2O_3 nanoparticles [31].

3.3 Chemical Composition Study

The EDS spectra of La_2O_3 NP samples with various PEG concentrationsand calcined at 750 °Care represented in Figure 9. The weight percentage (wt.%) of the different elements present in all samples are listed in Table 5. The results confirmed the presence of oxygen (O) as well as lanthanum (La) in agreement with previous work [34]. Some carbon was also present most likely due to the carbon adhesive tape used to secure the nanoparticle samples onto the SEM stabs.

3.4 Fourier Transform Infrared Spectroscopy analysis

The FTIR spectra collected in the wavenumber range 4000-400 cm^{-1} of La_2O_3 NPs with different PEG-concentrations are illustrated in Figure 10. From Figure 10, a broad band (identified as A) observed at 3424, 3421, and 3424 cm^{-1}, due to different PEG-contents, shows the presence of O-H stretching vibration which is due to the absorbed moisture on the nanoparticle surfaces [36]. An absorption peak (identified as B)detected at 1459, 1456, and 1460 $cm^{-1}$and a sharp absorption band (identified as C)seen at 1363, 1362 and 1363 cm^{-1} in the nanoparticle samples at PEG-contents, respectively originated from the asymmetric and symmetric stretching of COO^{-}

functional group [37]. Another band observed at 1067, 1067, and 1067 cm^{-1}(identified as D) is arisen due to C-O stretching vibration but in the same samples, however the sharp absorption band seen at 846, 845, and 845 cm^{-1}(identified as E) is owing to C-O bending vibration. The broad absorption band detected at 678, 676, and 678 cm^{-1}(identified as F) is assumed to occurdue to La-O stretching vibration, while the small band found at 509, 511, and 510 cm^{-1} (identified as G) is due to La–O bending vibration. The presence of these bands, therefore, confirmed the existence of La_2O_3 phase in the synthesized nanoparticles [38]. The location of band frequencies and corresponding modes of vibrations are recorded in Table 6.

3.5 Thermal analysis of La_2O_3 NPs

TG-DSC traces of the lanthanum compound dried gel powder, with various PEG-contents and calcined at 300 °Cin argon atmosphere, used to investigate the thermal decomposition are presented in Figure 11. Figure 11 shows four different regions indicated by letters A, B, C, and D. These regions are indication of different weight losses of the nanoparticles at different range of temperatures. A total of 2.25 % weight loss associated with region A is due to the removal of surface water from the nanoparticle samples. Due to the same aspect, a small endothermic peak in DSC curve was also observed at 90 °C. 7.25 % weight loss in the second region indicated by letter B is ascribed to the evaporation of the surfactant (PEG) which has a boiling point of 260 °C. The DSC trace also shows an intense endothermic peak in B region at 370 °C. The DSC trace in region C, between temperature 410 and 510 °C, shows an endothermic peak at 510 °C which corresponds to the oxidation of the residual organic compounds from PEG and the corresponding weight loss in TG curve was recorded to be 2 %. Finally, a 5.5 % weight loss in region D was associated with the final decomposition of lanthanum compounds. Consequently, an endothermic peak at 750 °C in DSC curve is obtained in region D [31].

3.6 Photoluminescence (PL) studies

The photoluminescence (PL) spectra of La_2O_3 NPs synthesized with various PEG-contents are demonstrated in Figure 12. From Figure12, it is seen that the strongest emission band is located at a wavelength of 364 nm for all the nanoparticle samples. The observed emission band at 364 nm is a typical green band. This is believed to be the recombination of a delocalized electron near the conduction band with a single charged state of a surface oxygen vacancy [39]. The higher fluorescence intensity of the La_2O_3 sample is an indication of the higher surface-to-volume ratio and higher density of single ionized oxygen vacancies, resulting from the small particle size. A small band is also observed at 465 nm for all samples. Our findings were consistent with the suggestions presented by G. Wang *et al.* [40].

4. Conclusions

La_2O_3 nanoparticles successfully synthesised *via* a simple sol-gel technique at various PEG concentrations were studied. XRD datashowed that the diffraction peaks of La_2O_3 NPs can be indexed to (100), (002), (101), (102), (110),(200), (112), and (201) reflection planes corresponding to hexagonal phase with lattice constant values of $a = b = 0.3973$ nm and $c = 0.6129$ nm. The average crystal size calculated by Debye Scherrer's equation was found to be in the range of 18.14-33.26 nm. The average particle size estimated from ESEM micrographs for different dispersed La_2O_3 NPs samples with various PEG concentrations were in the range of 41.0-34.1 nm. The La_2O_3 nanoparticle size was decreased with increasing concentration of the PEG. The EDS study confirmed the presence of oxygen and lanthanum in the synthesized nanoparticles. FTIR spectroscopy suggested that all samples exhibited a broad band in the range of 3451-3417 cm^{-1} associated with O-H stretching vibrations in absorbed water molecules. La-O stretching and bending vibrations were detected in the wavenumber range of 730-638 cm^{-1} and 514-509 cm^{-1}, respectively. TGA-DSC curves showed three main thermal transitions associated with the weight loss phenomena. The weight losseswere accompaniedby the evaporation of the surfactant PEG, the oxidation of the residual organic compounds from the PEG and the decomposition of lanthanum compounds. The PLspectra of different La_2O_3 NP samples presented a strong emission band located at the wavelength of 364 nm, typical green band for all samples.

Acknowledgments

The financial support of Bangladesh Government under Bangabandhu Fellowship Program to carry out the MRes studies at School of Metallurgy and Materials, University of Birmingham, UK is gratefully acknowledged by H. Kabir. H. Kabir and M. Mahbubur Rahman also thankfully acknowledge Jahangirnagar University for providing with the adequate supports and facilities to carry out this work.

References

[1] P. Huang, J. Li, S. Zhang, C. Chen, Y. Han, N. Liu, Y. Xiao, H. Wang, M. Zhang, Q. Yu, Y. Liu, and W. Wang, Effects of lanthanum, cerium, and neodymium on the nuclei and mitochondria of hepatocytes: Accumulation and oxidative damage, Environ. Toxicol. Pharmacol. 31 (2011) 25–32.

[2] C. V. Reddy, I. N. Reddy, J. Shim, D. Kim, K. Yoo, Synthesis and structural, optical, photocatalytic, and electrochemical properties of undoped and yttrium-doped tetragonal ZrO_2 nanoparticles, Ceramics International, 44 (11) (2018) 12329-12339.

[3] S. Y. Liu, Y. Cai, X. Y. Cai, H. Li, F. Zhang, Q. Y. Mu, Y. J. Liu, Y. D. Wang, Catalyzed degradation Congo red in the aqueous solution by $Ln(OH)_3$ (Ln¼Nd, Sm, Eu, Gd, Tb, and Dy) nanorods, Appl.Catal. A4 53(2013) 45–53.

[4] J. Liu, G. Wang, L. Lu, Y.Guoand L. Yang, Facile shape-controlled synthesis of lanthanumoxide with different hierarchical micro/nanostructures for antibacterial activity based on phosphate removal, RSC Adv. 7 (2017), 40965-40972.

[5] G. Kalpana, J. Varuna, P. Sanjeevi, M. Elango, Influence of Mg concentration on structural, morphological and optical properties of nanoceria, Ceramics International, 44 (10) (2018) 11820-11827.

[6] C. Bouzigues, T. Gacoin, and A. Alexandrou, Biological Applications of Rare-Earth Based Nanoparticles, ACS Nano 5 (2011) 8488–8505.

[7] Y. Gao, Y. Masuda, and K. Koumoto, Micropatterning of lanthanum-based oxide thin film on self-assembled monolayers, J. Colloid Interface Sci. 274 (2004) 392–397.

[8] J. Xie, Y. Lin, C. J. Li, D. Y. Wu and H. N. Kong, Removal andrecovery of phosphate from water by activated aluminium oxide and lanthanum oxide, Powder Technol. 269 (2015) 351-357.

[9] L. Yulin, Y. Jun, L. Xiaoci, H. Weiya, T. Yu, Z. Yuanmin, Combustion synthesis and stability of nanocrystalline La_2O_3 via ethanolamine-nitrate process, J. Rare Earths 30, (2012) 48–52.

[10] S. Khanjani and A. Morsali, Synthesis and characterization of lanthanum oxide nanoparticles from thermolysis of nanostructured supramolecular compound, J. Mol. Liq. 153 (2010) 129–132.

[11] B. P. Gangwar, V. Palakollu, A. Singh, S. Kanvah, S. Sharma, Combustion synthesized La_2O_3 and $La(OH)_3$: recyclable catalytic activity towards Knoevena gel and Hantzschre actions, RSC Adv. 4 (2014) 55407–55416.

[12] M. Sasidharan, N. Gunawardhana, M. Inoue, S. Yusa, M. Yoshio, K. Nakashima, La_2O_3 hollow nano-spheres for high performance lithium-ion rechargeable batteries, Chem. Commun. 48 (2012) 3200–3202.

[13] V. M. Lebarbier, D. Mei, D. H. Kim, A. Andersen, J. L. Male, J. E. Holladay, R. Rousseau, Y. Wan, Effects of La_2O_3 on the mixed higher alcohols synthesis from syngas over Co catalysts: a combined theoretical and experimental study, J. Phys. Chem. C115 (2011) 17440–17451.

[14] S. Jafari Nejad, H. Abolghasemi, M. a. Moosavian, A. Golzary, and M. G. Maragheh, Fractional factorial design for the optimization of hydrothermal synthesis of lanthanum oxide nanoparticles under supercritical water condition, J. Supercrit. Fluids 52 (2010) 292–

297.

[15] J. Kang, Y. Kim, D. W. Cho, Y. Sohn, Synthesis and physicochemical properties of $La(OH)_3$ and La_2O_3 nanostructures, Mater. Sci. Semicon. Proces. 40 (2015) 737–743.

[16] B. Tang, J. Ge, C. Wu, L. Zhuo, J. Niu, Z. Chen, Z. Shi, and Y. Dong, Sol–solvothermal synthesis and microwave evolution of $La(OH)_3$ nanorods to La_2O_3 nanorods, Nanotechnol. 15 (2004) 1273–1276.

[17] M.A. Shadiya, N. Nandakumar, R. Joseph, K.E. George, On the facile polyvinyl alcohol assisted sol-gel synthesis of tetragonal zirconia nanopowder with mesoporous structure, Adv. Powder Technol. 28 (2017) 3148-3157.

[18] A. V. Murugan, S. C. Navale, V. Ravi, Synthesis of nanocrystalline La_2O_3 powder at 100 °C, Mater. Lett. 60 (2006) 848–849.

[19] M. Salavati-Niasari, G. Hosseinzadeh, and F. Davar, Synthesis of lanthanum hydroxide and lanthanum oxide nanoparticles by sonochemical method, J. Alloys Compd. 509 (2011) 4098–4103.

[20] M. Ranjbar, M. Yousefi, Synthesis and Characterization of Lanthanum Oxide Nanoparticles from Thermolysis of Nano-sized Lanthanum (III) Supramolecule as a Novel Precursor, J. Inorg. Organomet. Polym. 24 (2014) 652–655.

[21] Q. Zhou, H. Zhang, F. Chang, H. Li, H. Pan, W. Xue, D.Y. Hu, S. Yang, Nano La_2O_3 as a heterogeneous catalyst for biodiesel synthesis by transesterification of Jatropha curcas L. oil, J. Indust. Eng. Chem. 31(2015) 385–392.

[22] M. A. Farrukh, F. Imran, S. Ali, M. K. Rahmanand I. I. Naqvi, Micelle Assisted Synthesis of La_2O_3 Nanoparticles and Their Applications in Photodegradation of Bromophenol Blue, Russian J. Appl. Chem. 88 (2015) 1523−1527.

[23] E. K. Goharshadi, T. Mahvelati, and M. Yazdanbakhsh, Influence of preparation methods of microwave, sol–gel, and hydrothermal on structural and optical properties of lanthania nanoparticles, J. Iran. Chem. Soc. 13 (2016) 65–72.

[24] S. Khanahmadzadeh, N. Paknahad, FarinazAzizi, Synthesis, characterization and photocatalytic activity of the lanthanum barium copper oxide nanoparticles in presence of stearic acid as solvent and stabilizer agent, J. Mater. Sci: Mater Electron 28 (2017) 2747-2753.

[25] J. Liu, G. Wang, L. Lu, Y. Guo and L. Yang, Facile shape-controlled synthesis of lanthanum oxide with different hierarchical micro/nanostructures for antibacterial activity based on phosphate removal, RSC Adv. 7 (2017) 40965-40972.

[26] L. Zhang, L. Zhou, Q. X. Li, H. Liang, H. Qin, S. Masutani, B. Yoza, Toxicity of lanthanum oxide nanoparticles to the fungus Moniliellawahieum $Y12^T$ isolated from biodiesel, Chemosphere, 199 (2018) 495-501.

[26] M. Moothedan, K.B. Sherly, Synthesis, characterization and sorption studies of nano lanthanum oxide, J. Water Process Engi. 9 (2016) 29–37.

[27] G. Z. Jia, Y. F. Wang, and J. H. Yao, Fabrication and strain investigation of ZnO nanorods on Si composing sol-gel and chemical bath deposition method, J. Phys. Chem. Solids. 73 (2012) 495–498.

[28] C. Hu, H. Liu, W. Dong, Y. Zhang, G. Bao, C. Lao, Z. L. Wang, $La(OH)_3$ and La_2O_3 Nanobelts-Synthesis and Physical Properties, Adv. Mater. 19 (2007) 470–474.

[29] B. D. Cullity, Elements of X-ray Diffraction, Second Ed., Addison-Wesley Company, USA, 1978.

[30] R. Jenkins, R. L. Snyder, Chemical Analysis: Introduction to ray Powder Diffractometry, John Wiley & Sons, Inc., New York, 1996.

[31] X. Wang, M. Wang, H. Song, B. Ding, A simple sol-gel technique for preparing lanthanum oxide nanopowders, Mater. Lett.60 (2006) 2261–2265.

[32] R. John, and R. Rajakumari, Synthesis and Characterization of Rare Earth Ion Doped Nano ZnO, Nano-Micro Lett. 4 (2012) 65-72.

[33] F. Ozutok, B. Demirselcuk, E. Sarica, S. Turkyilmaz, V. Bilgin, Study of Ultrasonically Sprayed ZnO Films: Thermal Annealing Effect, Acta Phys. Polonica.A, 121 (2012) 53-55.

[34] A. Manikandan, E. Manikandan, B. Meenatchi, S. Vadivel, S.K. Jaganathan, R. Ladchumananandasivam, M. Henini, M. Maaza, J.S. Aanand, Rare earth element (REE) lanthanum doped zinc oxide (La: ZnO) nanomaterials: Synthesis structural optical and antibacterial studies, J. . Alloys and Comp. 723 (2017) 1155-1161.

[35] D. Dickson, G. Liu, C. Li, G. Tachiev, Y. Cai, Dispersion and stability of bare hematite nanoparticles: Effect of dispersion tools, nanoparticle concentration, humic acid and ionic strength, Sci. Total Environ. 419 (2012) 170–177.

[36] G. Zou, R. Liu, W. Chen, Z. Xu, Preparation and characterization of lamellar-like $Mg(OH)_2$ nanostructures via natural oxidation of Mg metal in formamide/water mixture, Mater. Res. Bull. 42 (2007) 1153–1158.

[37] T. Takei, I. Okuda, K. K. Bando,T. Akita, M. Haruta, Gold cluster supported on $La(OH)_3$ for CO oxidation at 193K, Chem. Phys. Lett. 493 (2010) 207–211.

[38] K. Bikshalu, V. S. K. Reddy, P. C. S. Reddy, K. V. Rao, Synthesis of La_2O_3 Nanoparticles by Pechini Method for Future CMOS Applications, *IJEAR* 4 (2014) 12-15.

[39] N. Zhang, R. Yi, L. Zhou, G. Gao, R. Shi, G. Qiu, X. Liu, Lanthanide hydroxide nanorods and their thermal decomposition to lanthanide oxide nanorods, Mater. Chem. Phys. 114 (2009) 160–167.

[40] G. Wang, Y. Zhou, D. G. Evans, and Y. Lin, Preparation of Highly Dispersed Nano-La_2O_3 Particles Using Modified Carbon Black as an Agglomeration Inhibitor, Ind. Eng. Chem. Res. 51 (2012) 14692−14699.

e-component

Click here to download e-component: Graphical Abstract.docx

e-component

Click here to download e-component: Highlights.docx